Optimization of Electric Thrusters for Primary Propulsion Based on the Rocket Equation*§

Monika Auweter-Kurtz, Helmut Kurtz
Institut für Raumfahrtsysteme, Universität Stuttgart
Pfaffenwaldring 31
70550 Stuttgart
Germany
Tel.: +49(711)685-2378
Fax: +49(711)685-7527
auweter@irs.uni-stuttgart.de, kurtz@irs.uni-stuttgart.de

IEPC-01-181

During the last decade, electric propulsion systems have been established for orbit maintenance of satellites. More than 150 spacecrafts are now equipped with almost 400 thrusters for this purpose. The current decade will see the use of electric propulsion for primary propulsion. The purpose of this paper is to determine optimal mission parameters for these tasks. Depending on the mission profile, ion thrusters, Hall thrusters, thermal arcjets or MPD thrusters are preferable. All electric propulsion systems have in common that they can be operated in a wide range of the specific impulse and that the thrust efficiency and therefore also the specific power of the propulsion system depend strongly on the specific impulse. The optimal specific impulse for a particular mission depends, therefore, on the kind of thruster and the chosen propellant. This paper shows that for MPD, ion, Hall ion and thermal arcjet thrusters the optimal specific impulse for a particular mission can be determined by an optimization which is based on the rocket equation. Using, in addition, a simple cost function, the influence of the cost factors is explained. Finally, the results for a few missions for which electric propulsion systems for primary propulsion have been selected are discussed.

Nomenclature

a	[m/s]	parameter
b	[s/m]	parameter
c_e	[m/s]	effective exhaust velocity
e	[C]	elementary charge
f,f_1		functions
g		function
$g_{I,II}$		examples of function g
k		factor
$\dot{m}$	[kg/s]	propellant flow rate
m_{LS}	[kg]	payload & structure mass
m_0	[kg]	initial vehicle mass
m_P	[kg]	propellant mass for achieving mission
m_{PS}	[kg]	propulsion system dry mass (incl. power supply)
Pel	[W]	electrical power
T	[N]	thrust
TR	[s^{-1}]	transport rate
v_A	[m/s]	Alfvèn velocity
E	[J/kg]	specific energy
Δv	[m/s]	velocity increment for mission
α_F	[W/kg]	spec. power of propulsion system
α_{PS}	[W/kg]	specific power of power supply

*Presented as Paper IEPC-01-181, 27th International Electric Propulsion Conference, Pasadena, CA, 15-19 October, 2001.

η_{PC}	efficiency of power conditioner
η_T	thrust efficiency
$\eta_{T,\,max}$	maximum (theoretical) thrust efficiency
μ_{LS}	payload and structure mass fraction
τ [s]	trip time
$\tau^*_{I,II}$	normalized trip time

Introduction

Nowadays it is no longer questionable that electric propulsion systems are serious competitors for primary propulsion with respect to orbit transfer, moon or interplanetary missions. Depending on the mission profile, different electric thruster types (thermal arcjets, MPD, ion and Hall ion thrusters) are being discussed, have been investigated or developed and some have even been space-proofed for these purposes.[1-5]

Since the early 70s, the advantages and disadvantages of electric propulsion versus chemical propulsion for transfer missions have been discussed in many papers,[6,7] as well as the comparison between the different types of electric thrusters.[7-11] In general, only the rocket equation in these papers is varied and applied to different thruster types and different mass distributions, without special regard to optimizations.

All of the thruster types taken into consideration have in common that the effective exhaust velocity can vary greatly, whereby, however, the thruster efficiency then also changes. In this paper, for each thruster type and appropriate propellant the optimal effective exhaust velocity for a certain velocity increment of the mission will be ascertained. The flight time at a maximum payload capacity should be as low as possible. In the older, valuable works of Langmuir,[12] Irving,[13] and Stuhlinger[14] and in a USAF study,[15] such optimizations have already been made, though under the assumption of a constant specific power α_F of the propulsion system. However, the specific power

$$\alpha_F = \eta_{PC}\,\eta_T(c_e)\,\alpha_{PS} \qquad (1)$$

depends on the efficiency of the power conditioning unit η_{PC}, the specific power of the power system α_{PS} and the thruster efficiency η_T. α_{PS} is defined as the ratio of electrical power and the sum of power supply mass, power conditioner mass, and motor mass. While η_{PC} and the specific power of the system α_{PS} can be seen as independent of the specific impulse as long as the motor mass is much lower than the power supply mass, this is not the case for the thruster efficiency η_T. For all the electrical thrusters considered here, the thruster efficiency and therefore also α_F strongly depend on the effective exhaust velocity c_e. Therefore, it is absolutely necessary to introduce this dependency into the rocket equation for optimization purposes. This has already been done and published in a previous paper[16] and it was shown that the Langmuir-Irving Optimization[12,13] is a borderline case.

Since the costs of orbital mass transfer are not only determined by the amount of payload but also by the transfer time, a transport rate has been defined and is included in the optimization. Especially for manned missions the trip time should be minimized not only because of cost but also for safety reasons. In the previous paper,[16] an instrument was provided for a quick evaluation of the optimal range of the thruster parameters for a certain mission profile for ion and MPD thrusters. During the last ten years, Hall ion thrusters and thermal arcjets have also shown performance data which make them interesting candidates as primary propulsion systems.[4, 17] Therefore, within this paper it is shown that the methods which have already been developed for ion and MPD thrusters can also be applied for Hall ion thrusters and high power thermal arcjets. For three examples of recent missions Deep Space 1,[1] SMART-1[2] and MUSES-C[3] the predicted optimal effective exhaust velocity is compared to the values for which the selected thrusters have been qualified. A new method for thermal arcjet thrusters is also introduced.

Optimization Based on the Rocket Equation

For the evaluation of a thruster system, the attainable velocity increment is of great interest. The

connection between the attainable velocity increment Δv, the required flight time τ, the payload and structure fraction μ_{LS} on the one hand and the propulsion system characterized by the effective exhaust velocity c_e and specific power α_F on the other hand is provided by the rocket equation. For rockets with energy sources separate from the propellant, i.e. mainly electrical thrusters, it can be written in dimensionless form:

$$\frac{\Delta v}{c_e} = \ln\left[\frac{1+\frac{c_e^{\,2}}{2a_F t}}{m_{LS}+\frac{c_e^{\,2}}{2a_F t}}\right] \qquad (2)$$

where $\sqrt{2a_F t}$ is a characteristic velocity which can be derived from the specific energy ε of the propulsion system ($\varepsilon=\alpha_F\tau$).[18] The payload and structure mass fraction is defined as $\mu_{LS} = m_{LS}/m_O$ with m_0 as initial mass of the spacecraft and m_{LS} as sum of the payload and structure mass. To compare electric propulsion systems with chemical rockets the total mass is divided as follows:

$$m_0 = m_{LS} + m_{PS} + m_P \qquad (3)$$

with the propellant mass m_P, and the mass of the propulsion system including the power system m_{PS}.

The propulsion system has to be optimized so that a maximum payload mass fraction μ_{LS}, a minimum flight time τ and a maximum velocity increment Δv can be achieved. To obtain the conditions for these requirements, the rocket equation 2 is solved for μ_{LS}, τ and Δv respectively and partially differentiated with respect to the exhaust velocity c_e. An investigation of the second derivation revealed that, as required, a maximum and a minimum are being dealt with respectively. By substituting the rocket equation 2 into all three equations obtained, they can be brought into the same form.[16] This signifies that the minimal flight time, maximal payload fraction and maximal velocity increment yield one and the same condition and are, therefore, reached at the same time. Furthermore, in this condition, the term dependent on the specific power α_F can be separated, i.e. it can be represented in the form g=f, where g is a function only of α_F and c_e, whereas f is a function only of μ_{LS} and $\Delta v/c_e$:

$$\underbrace{\frac{c_e}{a_F}\frac{\partial a_F}{\partial c_e}}_{g} = \underbrace{2+\frac{\Delta v}{c_e}e^{\Delta v/c_e}\frac{m_{LS}-1}{\left(1-e^{\Delta v/c_e}\right)\left(m_{LS}e^{\Delta v/c_e}-1\right)}}_{f} \qquad (4)$$

The function f, which is independent of the propulsion parameter α_F, can be displayed with $\Delta v/c_e$ as an abscissa and with the payload and structure fraction μ_{LS} as a parameter, which is done in Fig. 1. From this figure it can be clearly seen that there is no optimization possible for f and g values between 1 and 2, respectively. For further discussion the function g has to be derived which is a function of the specific power of the propulsion system. The specific power α_F strongly depends on the thruster type and propellant choice.

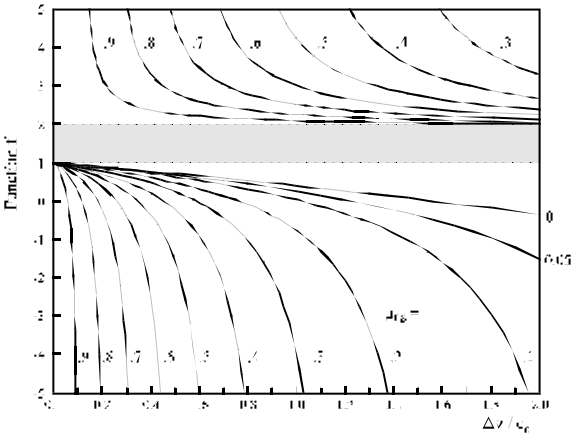

Fig. 1: Function f vs $\Delta v/c_e$ with the payload plus structure mass fraction μ_{LS} as parameter

High Power Thermal Arcjets, Ion, Hall Ion and MPD Thrusters

For ion, Hall ion and MPD thrusters as well as for high power thermal arcjets, the degree of ionization is close to one or at least constant within a wide range of operation. Consequently, the reaction losses of the beam do not significantly change. On the other hand, the thermal losses in these thrusters are low compared to the thrust power and to the other losses and/or do not significantly change. Therefore, the thrust efficiency η_T defined as thrust power divided by total power input can be approximated by the formula

$$\eta_T = \eta_{T,\max}\frac{c_e^{\,2}}{c_e^{\,2}+(kv_A)^2} \qquad (5)$$

used already by Stuhlinger for ion thrusters.[14] $\eta_{T,max}$ is an asymptotic value for $c_e \to \infty$ which includes primarily the thermal and the nozzle losses. The second factor on the right hand side of Eq. 5 represents the quotient of the kinetic energy of the beam divided by its enthalpy. The velocity v_A is called Alfvèn velocity. It is the average velocity a particle would reach in the case that the sum of the reaction energy, heat of fusion and heat of evaporation were changed into kinetic energy:

$$v_A = \sqrt{\frac{2e}{\overline{m}_A}\left(a_D E_D + \sum_i a_{I,i} E_{I,i}\right) + 2r_F + r_E} \qquad (6)$$

with $\overline{m}_A$: average atomic mass, α_D: degree of dissociation, $\alpha_{I,i}$: degree of ionization of the grade, E_D [eV]: dissociation energy, $E_{I,i}$ [eV]: averaged ionization energy of the i^{th} grade, r_F [J/kg]: specific heat of fusion, r_E [J/kg]: specific heat of vaporization. In Table 1 the Alfvén velocities for various propellants for full ionization (only first stage) are listed.

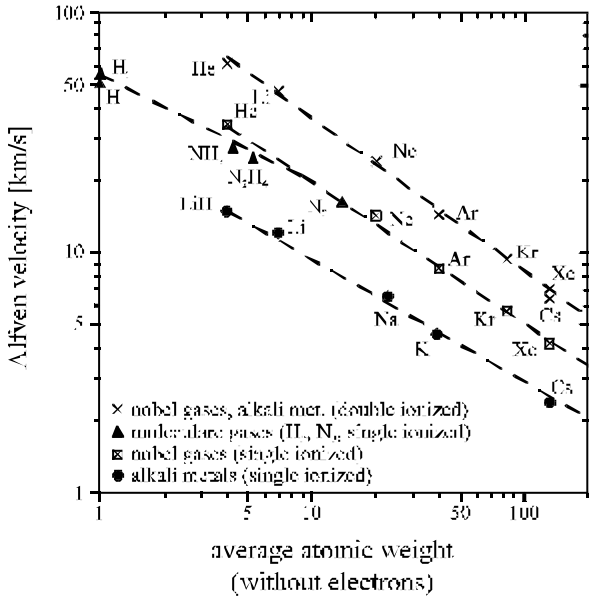

Fig. 2: Alfvèn velocity as function of the average atomic weight (without electrons)

In Fig. 2, it is clearly visible that the Alfvén velocity strongly depends on the average atomic mass and on its location within the periodic table of elements as it was found by Bühler.[19] Low values are achievable for high atomic masses and for alkali metals. For ion and Hall ion thrusters the atomic weight of the propellant should be as high as possible in order to achieve a high thrust level. In this case, as can be seen from Fig. 2, the Alfvén velocity is also lowest, which means the thrust efficiency or at least $\eta_{T,max}$ is high. In the case of MPD thrusters, the propellant selection is not dominated by the request to achieve a high thrust level but by the demand to increase the effective exhaust velocity and improve the thruster efficiency. For achieving high specific impulses, the average atomic weight of the propellant should be low with respect to the thermal thrust portion. The magnetic thrust portion does not depend on the propellant choice. For self-field MPD thrusters, it can be shown[18] that the effective exhaust velocity c_e is restricted to the Alfvén velocity, if the thermal thrust portion is low compared to the MPD thrust. Both imply the choice of a light-weight propellant. On the other hand, to improve the magnetic thrust the current I has to be as high as possible because the magnetic thrust is proportional to I^2. This means that the power has to be supplied at a low voltage. Therefore, propellants with low arc voltage levels are preferable. In order to achieve high efficiencies the Alfvén velocity should be low. Taking all these arguments into account, argon and also alkali metals are a good choice for MPD devices. Whether, for example, hydrogen is of interest depends mainly on the magnitude of the thermal thrust fraction. For thermal arcjets the atomic mass of the propellant should be as low as possible to achieve the highest specific impulses possible.[18] In order to maximize efficiency the current level of operation should be minimized because the anode loss, which is dominant for these devices, increases linearly with the current. Taking all these arguments into consideration, hydrogen, which offers a high voltage level, is the best propellant choice for thermal arcjets although its Alfvén velocity is the highest.

The factor k in the ansatz Eq. 5 makes it possible to consider the average losses which occur during the production of an ion in a certain thruster. The term kv_A, therefore, can be described as effective, "thruster specific" Alfvén velocity. A propulsion system consisting of a certain thruster and propellant is therefore characterized by $\eta_{T,max}$ and kv_A. Approximation 5 corresponds quite well to

Table 1: Molecular weights, ionization (E_I) and dissociation energies (E_D), heat of fusion r_F, heat of vaporization r_E and Alfvén velocity v_A (for complete first ionization) for the most important propellants

Propellant	Molecular mass		E_D [eV]	$E_{I,1}$ [eV]	$E_{I,2}$ [eV]	r_F [J/kg]	r_E [J/kg]	v_A [km/s]
	cold	fully diss.						
Hydrogen, H_2	2	1	2.26	13.59	-	$5.78*10^4$	$4.60*10^5$	55.1
Methane, CH_4	16	3.2	3.45	13.12	-	$5.86*10^4$	$5.48*10^5$	31.5
Helium, He	4	4	-	24.48	54.4	-	$2.09*10^4$	34.24
Ammonia, NH_3	17	4.25	3.04	13.83	-	$3.39*10^5$	$1.37*10^6$	27.63
Hydrazine, N_2H_4	32	5.33	3.06	13.9	-	$3.96*10^5$	$1.28*10^6$	24.75
Water, H_2O	18	6	3.2	13.6	-	$3.34*10^5$	$2.26*10^6$	23.28
Lithium, Li	6.94	6.94	-	5.39	75.62	$6.64*10^5$	$2.13*10^7$	13.76
Nitrogen, N_2	28.02	14.01	4.92	14.53	29.59	$2.57*10^4$	$1.99*10^5$	16.32
Oxygen, O_2	32	16	2.58	13.61	35.11	$1.38*10^4$	$2.13*10^5$	19.69
Sodium, Na	23	23	-	5.14	47.29	$1.13*10^5$	$5.86*10^6$	7.00
Potassium, K	39.1	39.1	-	4.34	31.81	$5.96*10^4$	$2.29*10^6$	4.87
Argon, Ar	39.95	39.95	-	15.76	27.62	$3.03*10^4$	$1.57*10^5$	8.72
Xenon, Xe	131.3	131.3	-	12.13	21.2	$2.34*10^4$	$9.63*10^4$	4.24
Cesium, Cs	132.91	132.91	-	3.89	25.1	$1.55*10^4$	$5.02*10^5$	2.58
Mercury, Hg	200.59	200.59	-	10.43	18.75	$1.17*10^4$	$3.01*10^5$	3.25

the measured efficiencies of plasma and ion engines.

In Fig. 3, some experimental results of MPD, ion, high power thermal arcjet and Hall ion engines approximated with Eq. 5 are plotted (see Table2). The experimentally verified areas are shown with a thick line. Introducing Eq. 5 into the left hand side of Eq. 4 one gets the function $g_I(kv_A,c_e)$ which is valid for ion, Hall ion and MPD thrust ers and high power thermal arcjets as a special case of $g(\alpha_F, c_e)$:

$$g_I = \frac{2}{1+\left(\frac{c_e}{kv_A}\right)^2} = \frac{2}{1+\left(\frac{c_e}{\Delta v}\right)^2\left(\frac{\Delta v}{kv_A}\right)^2} \quad (7)$$

Plotted against $\Delta v/c_e$ with the thruster type and mission dependent parameter $kv_A/\Delta v$, one obtains the set of curves displayed together with the function f in the upper part of Fig. 4.

The solutions for an optimized thruster are the points $f=g_I$. Due to the limitations of g_I: $0 \le g_I \le 2$ and the lack of f-values in the region $1<f<2$. The optimization is limited to 0 f, $g_I<1$. Furthermore,

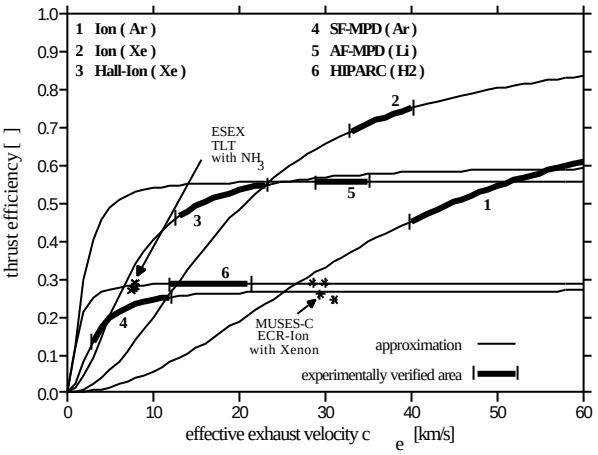

Fig. 3: Thruster efficiency vs. effective exhaust velocity for different thrusters (see Table 2)

from Fig. 4 it is obvious that $\Delta v/c_e$ is in general also restricted and with increasing $kv_A/\Delta v$ the area of $\Delta v/c_e$, in which an optimization is possible, gets smaller. Another important result can be derived: with an increasing dependency of $\eta_T(c_e)$, i.e. with rising $kv_A/\Delta v$ for a given mission, the optimal specific impulses become greater. The corresponding flight time of a mission can be achieved by introducing the ansatz Eq. 5 into the optimization condition 4 and using the rocket

equation 2 for eliminating the payload and structure mass fraction. By introducing a normalized flight time

$$\tau_I^* = \eta_{PC}\,\alpha_{PS}\,\eta_{T,max}\,\frac{\tau}{\Delta v^2} \qquad (8)$$

we achieve

$$t_I^* = \left\{\frac{c_e}{\Delta v}\left(1-e^{\Delta v/c_e}\right)\left[\frac{1}{1+\left(c_e/\Delta v\right)^2\left(\Delta v/kv_A\right)^2}-1\right]-\frac{1}{2}\right\} \qquad (9)$$
$$\cdot\left[\left(\frac{c_e}{\Delta v}\right)^2+\left(\frac{kv_A}{\Delta v}\right)^2\right]$$

Equation 9 shows that the normalized flight time τ_I^* is only a function of $\Delta v/c_e$ and $kv_A/\Delta v$ and can therefore be integrated into Fig. 4.

Figure 4 describes the field of all possible optimal values for a certain mission in the case of an ion, a Hall ion, an MPD propulsion or a high power thermal arcjet system in the form of a nomograph. With a given thruster type, i.e. with a given kv_A and $\eta_{T,max}$, a given power supply with α_{PS} andη_{PC}, and a given mission, i.e. Δv, the optimal exhaust velocity c_e and the minimal flight time τ can be determined for a certain payload fraction, for example.

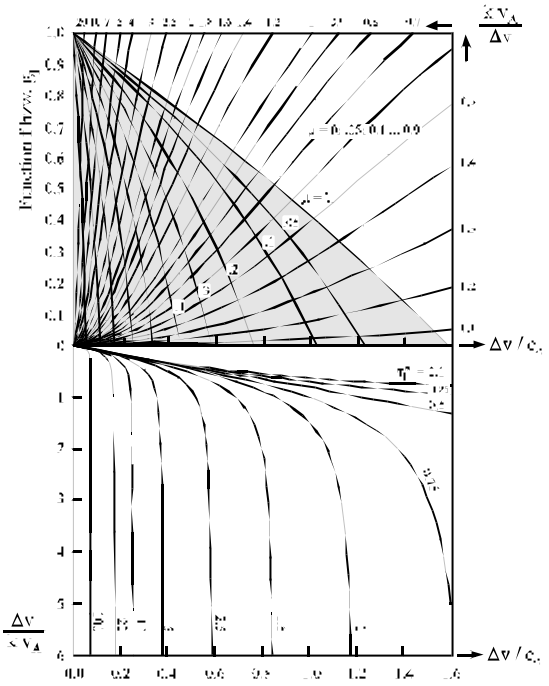

Fig. 4: Nomograph of the quantities Δv, t_I^*, m_{LS}, and c_e for the optimized rocket equation for high power thermal arcjets, ion, Hall ion and MPD thrusters

Thermal Arcjet Thrusters

Beside the case of the high power thermal devices which have already been discussed in the previous section, the degree of ionization and also the fraction of the thermal losses of a thermal arcjet change by varying the effective exhaust velocity c_e. Therefore the ansatz Eq. 5 cannot be used. But for thermal arcjets the effective exhaust velocity c_e is a linear function of the specific power $P_{el}/\dot{m}$ within a wide range of operation. Therefore, in this case the ansatz can be made

$$c_e = a + b\left(P_{el}/\dot{m}\right) \quad . \qquad (10)$$

Parameter a represents an exit velocity which corresponds to the energy content of the propellant which is not directly influenced by the arc. In the case of a thruster which is not regeneratively cooled, a corresponds to the cold gas thrust and

Table 2: Different thruster types and propellants [with approx. (5)]

Thruster	Propellant	kv_a [km/s]	v_a [km/s]	k [-]	$\eta_{T,max}$ [-]	c_e area exp. verified[km/s]	Ref.
ION	Ar	36,99	8,72	4,242	0,84	40-60	20
ION	Xe	19,67	4,24	4,639	0,93	30-40	20
SPT	Xe	7,01	4,24	1,653	0,6	13-23	21
SF-MPD	Ar	3,06	8,72	0,351	0,27	3-11	5
AF-MPD	Li	1,88	13,76	0,137	0,56	29-35	22,23
HIPARC	H_2	1,199	55,1	0,022	0,29	12-21	4

therefore increases as the size of the thruster and the power level increase. With increasing regenerative capacity of the thruster which is the highest for Marc 6 and with increasing heat capacity of the propellant, a also increases (see Table 3).
The parameter b represents the incline of the curves in Fig. 5. It depends greatly on the one hand on the propellants which can be seen from curves 1-3 being highest for hydrogen which offers high exit velocities even at low specific power levels. In the case of NH_3 or N_2H_4 the curves are steeper due to the greater improvement

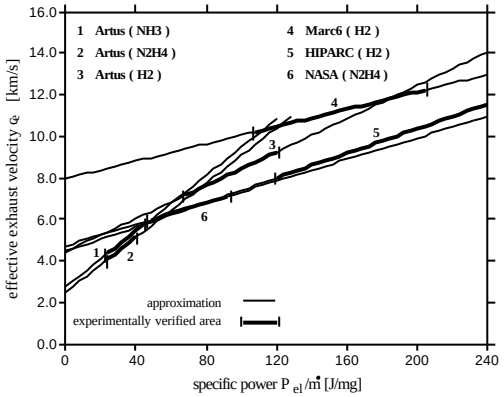

Fig. 5: Effective exhaust velocity c_e as function of specific power for different thermal arcjet thrusters and propellants (see Table 3)

during dissociation. For these two propellants b differs only slightly because it is very close to the Alfvén velocity. b generally increases with increasing Alfvén velocity and decreasing molecular weight because c_e strongly depends on the effective molecular weight. On the other hand, an increase of the regenerative cooling capacity makes b smaller which is obvious from the very low value of Marc 6.
For the thrust efficiencies using ansatz 10

$$h_T = \frac{T^2}{2\dot{m}P_{el}} = \frac{c_e^{\,2}}{2P_{el}/\dot{m}} = \frac{b}{2}\,\frac{c_e^{\,2}}{c_e - a} \qquad (11)$$

follows.
In Fig. 5 the effective exhaust velocity c_e of different arcjets listed in Table 3 is plotted against the specific power. Figure 5 makes it clear that the effective exhaust velocity increases with the increasing thruster size due to an increase of specific power. The HIPARC thruster is optimal for high power levels (100 kW). Only for the low power level can it be handled with ansatz 10. For high power operation ansatz 5 has to be applied. This part is included in the previous section. For the power levels shown in this section, it has to be recognized that the thrusters are not optimized.
Figure 6 shows the thrust efficiencies calculated for these propulsion systems. The experimentally verified area is plotted with a thick line, the thin line represents the curves which are obtained by using ansatz 10 and Eq. 11. The linear ansatz fits into the experimental results very well beside the very low and very high c_e region for a certain thruster. The very low values are not of any technical interest. At very high c_e-values, the fact that c_e no longer increases with rising specific power in a linear manner is a sign that the gas is nearly fully dissociated and in addition the fraction of ionization is no longer increasing at the same rate as it does in the lower c_e area. For high power

Table 3 Various thermal arcjet thrusters [with ansatz (10) in the case of HIPARC only the data for medium power operation (<39kW) is included here]

Thruster	Propellant	a [km/s]	b [s/km]	Experimentally verified c_e area [km/s]	Experimentally verified P_{el} area [W]	Ref.
ATOS-2	NH_3	2,75	6,74E-02	4,3-5,6	900-1600	24
Artus	N_2H_4	2,49	6,60E-02	4,2-5,2	1000-1600	25
ARTUR	H_2	4,46	4,00E-02	7,2-9,3	1000-1800	24
Marc6	H_2	7,97	2,09E-02	10,2-12,2	5000-9150	24
HIPARC	H_2	4,44	2,97E-02	8-12	24000-39000	4
NASA	N_2H_4	4,74	2,60E-02	6-7,1	1000-2500	26

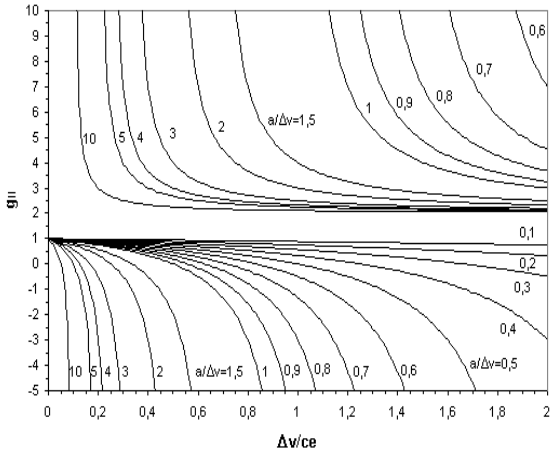

Fig. 7: Function of g_{II} vs. $\Delta v/c_e$ with the mission and propulsion system dependent parameter $a/\Delta v$

thermal arcjets the point can even be reached where as with MPD thrusters the gas is nearly fully ionized and the degree of ionization no longer changes by increasing c_e. In this case the behavior of the device can be handled using ansatz 5.

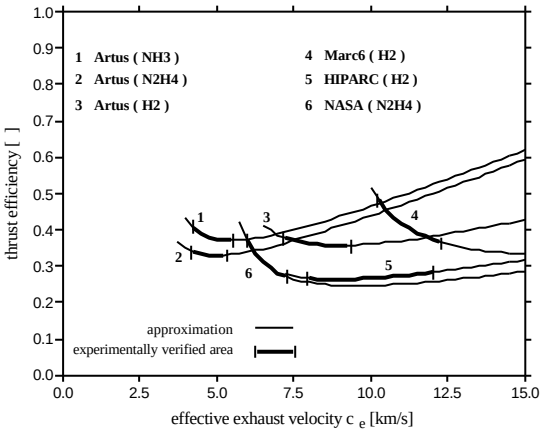

Fig. 6: Thrust efficiency η_T as function of effective exhaust velocity for different thermal arcjet thrusters and propellants (see Table 3)

Introducing Eq. 11 into the left hand side of the optimization condition in Eq. 4, the function g_{II} (a, c_e) can be obtained, which is valid for thermal arcjets in the boundaries discussed above:

$$g_{II}=\frac{c_e-2a}{c_e-a}=\frac{1-2\dfrac{a}{\Delta v}\dfrac{\Delta v}{c_e}}{1-\dfrac{a}{\Delta v}\dfrac{\Delta v}{c_e}} \quad . \qquad (12)$$

Plotted against $\Delta v/c_e$ with the propulsion system and mission dependent parameter $a/\Delta v$, one obtains the set of curves displayed in Fig. 7.

As in the case of the function f, no g_{II} values exist between 1 and 2. The function g_{II} becomes singular for $\Delta v/c_e=\Delta v/a$ or $c_e = a$. This point is not of any importance; only the region of $c_e>a$ is of interest because a corresponds to the effective cold gas thrust. Therefore, the upper part of Fig. 7 for $g_{II}\geq 2$ is not of any interest and one can concentrate on the region f,$g_{II}\leq 1$. In the upper part of the nomograph, the functions f and g_{II} are plotted with the payload and structure mass fraction μ_{LS} or rather $a/\Delta v$ as parameters. It can be seen from this figure that for a certain misison, i.e. Δv=const, the required optimal exhaust velocity $c_{e,opt}$, in order to even be able to conduct an optimization, increases with a and therefore with the thruster size.

As in the case of the thruster types in the previous section, a normalized trip time t^*_{II} can also be derived for thermal arcjet thrusters from the optimization condition 4 with respect to Eq. 12 using the rocket equation 2 for eliminating the payload and structure fraction μ_{LS}:

$$t^*_{II}=\frac{c_e}{\Delta v}\left[\frac{e^{\Delta v/c_e}-1}{\Delta v/c_e}+\frac{a}{\Delta v}\frac{\Delta v}{c_e}-1\right] \qquad (13)$$

with the normalized trip time defined as

$$t^*_{II}=h_{PC}a_{PS}\frac{b}{\Delta v}t \qquad (14)$$

From Eq. 13 follows that the normalized trip time is only a function of $a/\Delta v$ and $\Delta v/c_e$ and could therefore be integrated into the nomograph in Fig. 8. This nomograph describes the field of all possible optimal values for a certain mission in the case of a thermal arcjet propulsion system. With a given propulsion system, i.e. with given values a, b, α_{PS} and η_{PC} for a certain mission, i.e. Δv, the optimal exhaust velocity $c_{e,opt}$ and the minimal flight time τ_{min} can be determined for a certain payload fraction, for example.

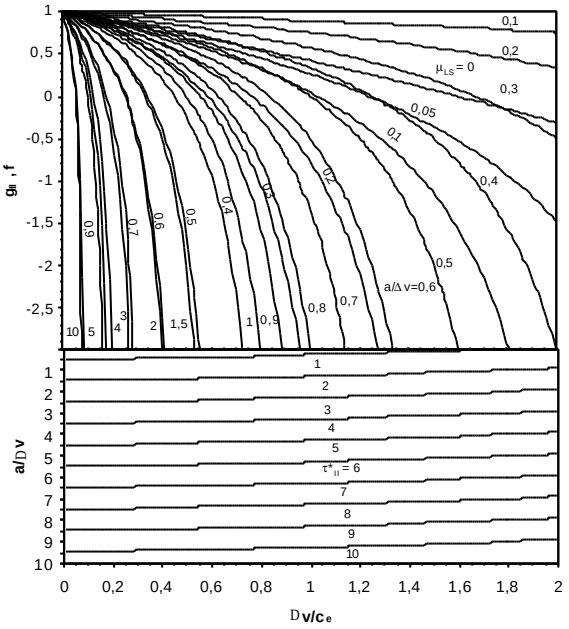

Fig. 8: Nomograph of the quantities Δv, τ^*, μ_{LS} and c_e for the optimized rocket equation for thermal arcjet thrusters

Optimization of a Transport Rate

Not only are the performance data of the propulsion system and the reliability important for missions, but ultimately the costs play a decisive role. An attempt will be made to model these costs with a relatively simply defined transport rate which should become maximum and to include this transport rate in the mission optimization.

If the payload and structure mass m_{LS} are related to the total propulsion mass at the onset of the mission (propulsion system mass m_{PS} plus propellant mass m_P) times flight time τ, one obtains the following definition of a transport rate:

$$TR = \frac{m_{LS}}{(m_{PS} + m_P)t} \quad . \qquad (15)$$

Using Eq. 3 the transport rate can be expressed as

$$TR = \frac{\mu_{LS}}{(1-\mu_{LS})\tau} \qquad (16)$$

which means that TR is only a function of the flight time τ and the payload and structure mass fraction μ_{LS}. Substituting τ in Eq. 16 with the rocket equation 2 provides TR as a function of μ_{LS}, c_e and Δv:

$$TR = \frac{2a_F m_{LS}\left(m_{LS} e^{\Delta v/c_e} - 1\right)}{c_e^{\,2}(1-m_{LS})\left(1-e^{\Delta v/c_e}\right)} \quad . \qquad (17)$$

Therefore, the necessary conditions for a maximal transport rate for a certain mission (Δv) are that the partial differentiations with respect to c_e and μ_{LS} be zero. Since the transport rate TR is only dependent on c_e over $\tau(c_e)$, the condition $\partial TR/\partial c_e$ is satisfied if $\partial\tau/\partial c_e = 0$. The resulting equation was deducted in the preceding section in the rocket equation optimization as Eq. 4. Since the specific power α_F is not a function of the payload fraction μ_{LS}, the condition $\partial TR/\partial\mu_{LS} = 0$ yields the following simple equation for the payload mass fraction μ_{LS}:

$$m_{LS} = 1 - \sqrt{1 - e^{-\Delta v/c_e}} \quad . \qquad (18)$$

For a given mission and propulsion system, the specific power α_F and the velocity increment Δv are fixed and the transport rate only depends on the exhaust velocity c_e and payload and structure mass fraction μ_{LS}. An investigation of the second derivative shows that the transport rate is maximal when both conditions are satisfied. Substituting Eq. 18 into Eq. 4 provides

$$\underbrace{\frac{c_e}{a_F}\frac{\partial a_F}{\partial c_e}}_{g} = 2 - \underbrace{\frac{(\Delta v/c_e)e^{\Delta v/c_e}\sqrt{1-e^{-\Delta v/c_e}}}{\left(1-e^{\Delta v/c_e}\right)\left[\left(1-\sqrt{1-e^{-\Delta v/c_e}}\right)e^{\Delta v/c_e}-1\right]}}_{f_{TR}} \qquad (19)$$

With the additional Eq. 18, the function $f = f_{TR}$ has become dependent only on $\Delta v/c_e$ and is no longer dependent on the mass fraction μ_{LS}, as in the case of the optimization of the rocket equation.

High Power Thermal Arcjets, Ion, Hall Ion and MPD Thrusters

It has been shown in the previous section that for high power thermal arcjets as well as for ion, Hall ion and MPD thrusters the function g becomes g_I (see Eq. 7). The function $f_{TR}(\Delta v/c_e)$ can now be plotted together with $g_I(\Delta v/c_e)$ with $kv_A/\Delta v$ as parameter which in contrast to $f(\Delta v/c_e, \mu_{LS})$ no longer represents a set of curves (see Fig. 10). So for a given propulsion system and mission the intersection of f_{TR} with g_I ($\Delta v/c_e$, $kV_A/\Delta v$) yields

one solution for an optimal specific impulse. According to Eq. 18, the function $\mu_{LS}(\Delta v/c_e)$ was also plotted into Fig. 9, so that one immediately obtains the corresponding payload mass fraction value μ_{LS}. In the same figure, the normalized flight time $\tau^*_{TR,I}(\Delta v/c_e)$ is displayed. The normalized flight time has been calculated with the use of Eqs. 1, 2, 7, 8, 18, and 19 as

$$t^*_{TR,I} = (c_e/\Delta v)^3 \left(e^{\Delta v/c_e} - 1\right) \sqrt{1 - e^{\Delta v/c_e}} \quad . \quad (20)$$

For a given mission Δv and a given propulsion system (kv_A, $\eta_{T,max}$, α_{PS}, η_{PC}), the exhaust velocity c_e, the payload and structure mass fraction μ_{LS} and the flight time τ can be determined from Fig. 9 and Eq. 8 so that the transport rate is optimal.

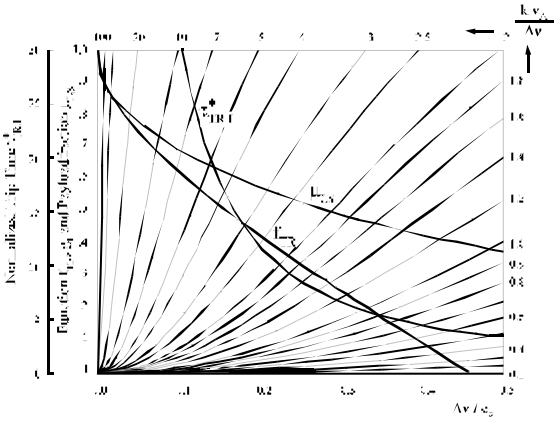

Fig. 9: Diagram of Δv, c_e, m_{LS}, and $t^*_{TR,I}$ for high power thermal arcjets, ion, Hall ion and MPD thrusters for the case of an optimized transport rate

Thermal Arcjet Thrusters

In the case of a thermal arcjet thruster the function g becomes g_{II} (see Eq. 12) which is plotted in a set of curves $g_{II}(\Delta v/c_e)$ in Fig. 7 with $a/\Delta v$ as parameter. In the same way as for the thrusters dealt with in the previous section, the functions $f_{TR}(\Delta v/c_e)$ (Eq. 19) μ_{LS} (Eq. 18) and $\tau^*_{TR,II}$ can be integrated in one graph. This is displayed in Fig. 10.

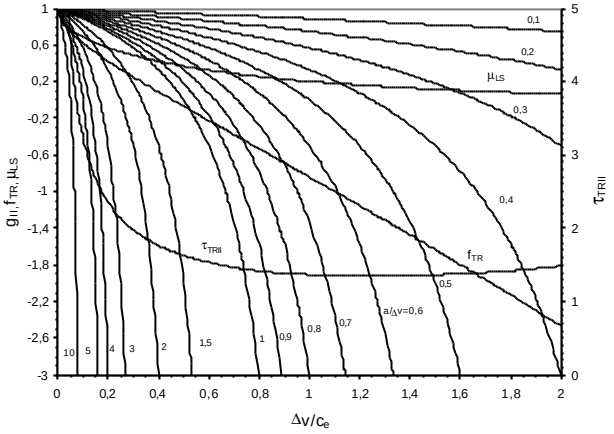

Fig. 10: Diagram of Δv, c_e, μ_{LS} and $\tau^*_{TR,II}$ for thermal arcjet thrusters for the case of an optimized transport rate

The normalized flight time $\tau^*_{TR,II}$ can be calculated from the optimization condition 18 substituting μ_{LS} with the help of the rocket equation 2 and using, in addition, the optimization condition 19 and Eqs. 12 and 14:

$$t^*_{TR,II} = \frac{\left(e^{\Delta v/c_e} - 1\right)\left[\left(1 - \sqrt{1 - e^{-\Delta v/c_e}}\right)e^{\Delta v/c_e} - 1\right]}{\left(\frac{\Delta v}{c_e}\right)^2 e^{\Delta v/c_e}\left[\sqrt{1 - e^{-\Delta v/c_e}} - 1\right]} \quad (21)$$

For a given mission Δv and a given thermal arcjet propulsion system (a, b, α_{PS}, η_{PC}), the exhaust velocity c_e, the payload and structure mass fraction μ_{LS} and the flight time τ can be determined from Fig. 10 and Eq. 14 so that the transport rate is optimal.

Comparison of Results for Different Thruster Types

In this section, the results of the different optimizations are compared for selected thruster types, which are listed in Tables 2 and 3. The corresponding efficiencies are displayed in Figs. 3 and 6. As power supply, a nuclear reactor like the SP-100[27] was selected with a specific power of α_{PS} = 33 W/kg. This reactor was chosen in regard to interplanetary missions. To allow for a better comparison, the same α_{PS} was also used as the basis for the thermal arcjet thrusters. This corresponds to a mean value for solar power supplies.

For all thrusters, the efficiency of the power conditioner was chosen with $\eta_{PC} = 0.9$.

Optimized Rocket Equation

Firstly, the results for the high power thermal arcjets, ion, Hall ion and MPD thrusters (Table 2) are shown. The optimized exhaust velocities c_e and the payload and structure mass fractions μ_{LS} for two velocity increments, Δv= 4km/s and 9km/s, as a function of the flight time, are shown in Figs. 11 and 12.

The optimal exhaust velocities c_e decrease with decreasing flight time τ (Figs. 11a and 12a). Furthermore, they decrease slightly with increasing velocity increment Δv. It is obvious that the optimal exhaust velocity not only strongly depends on the thruster type but also on the propellant. The difference between argon (No. 1) and xenon (No. 2) with the same ion thruster is more than 10km/s. It shows that the optimal exhaust velocities c_e depend not only on the maximum attainable thruster efficiency $\eta_{T,max}$ but also on the factor kv_A in ansatz 5, which is a sort of loss factor. The highest values result for the argon ion thruster (No. 1) and the lowest for the self-field MPD thruster (No. 4) and the high power thermal arcjet (No. 6), also with argon as the propellant. Both follow the same curve. But so far, the exhaust velocities of the SF-MPD thruster have only achieved the optimal value for low trip times. For long trip times an improvement of the c_e is required. In contrast, the high power thermal arcjet thruster shows optimal effective exhaust velocities for long trip times. The required optimal exhaust velocities are clearly higher for the AF-MPD thruster (No. 5) with lithium compared to the self-field device and it is even higher for the Hall ion thruster (No. 3) but clearly lower compared to the ion thruster with the same propellant (Xe). It is clearly visible that only for low velocity increments Δv and very long trip times can the optimal exhaust velocities be reached with an applied field MPD thruster with lithium as propellant. Over a wide range of missions the c_e-values attainable with this device are much too high. In comparison, the Hall ion thruster, the effective exhaust velocity is high enough only for short trip times. Besides the self-

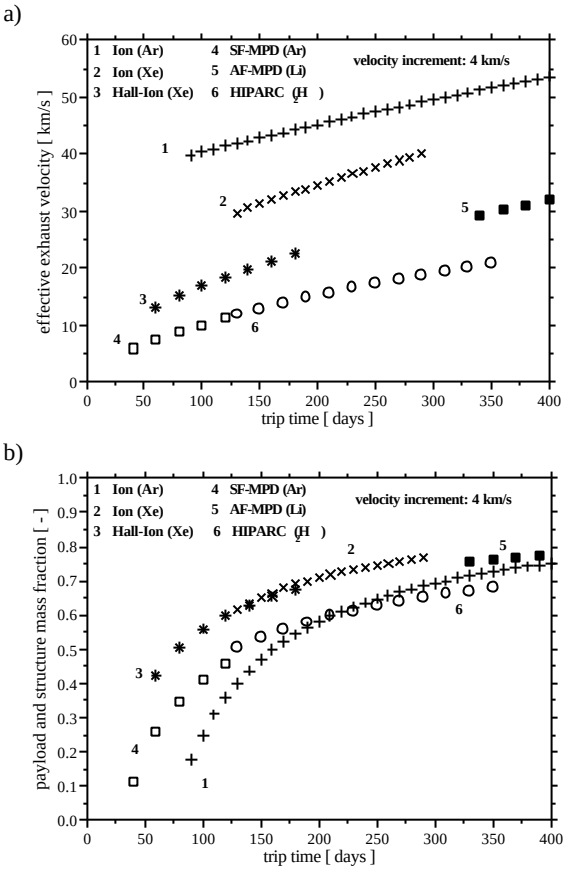

Fig. 11: Effective exhaust velocity c_e (a) , payload and structure mass fraction μ_{LS} (b) vs. flight time τ for thrusters in Table 2 for a velocity increment of Δv=4km/s

field MPD and the high power thermal arcjet, with optimal exhaust velocities c_e the thruster types are very distinct. This is not the case for the maximal payload and structure mass fraction μ_{LS}. The xenon ion and Hall ion thrusters both attain the best payload fraction because of their superior $\eta_{T,max}$ in the region of operation, the Hall ion thruster for the short trip times and the Xe ion thruster for the long trip times.

For the thermal arcjets (Table 3) the results for the same velocity increment (4 km/s and 9km/s) are displayed in Figs. 13 and 14.

It is apparent in Figs. 13 and 14 that for a specific Δv requirement for every thruster an optimal exhaust velocity can be given only within a small flight time area. This flight time area shifts for a

specific thruster with increasing Δv towards longer flight times. It can also be shown that the optimal effective exhaust velocity increases as the Δv requirement increases.[28] It can essentially

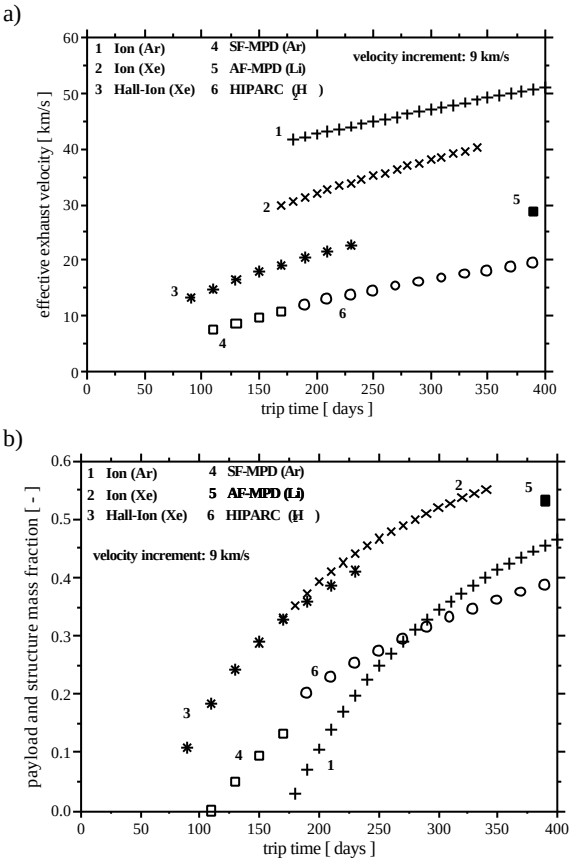

Fig. 12: Effective exhaust velocity c_e (a) , payload and structure mass fraction μ_{LS} (b) vs. flight time τ for thrusters in Table 2 for a velocity increment of Δv=9km/s

be remarked that due to the flat τ_{II}* curves, uncertainties in determining parameter a have a strong influence on c_{eopt} (see Fig. 8).

Optimization for a Transport Rate

The results for the optimization of the transport rate for the six selected thrusters in Table 2 are displayed in Fig. 15 as a function of the velocity increment Δv. The picture of the results compared to those of the optimization of the rocket equation has changed completely: the optimal exhaust velocities c_e increase with rising Δv (Fig. 15a) and asymptotically approach the optimization boundary, which is determined by the intersection of the f_1 curve with the abscissa in Fig. 9. The minimal exhaust velocities given by the optimization procedure and which would be attained at Δv=0 are equal to the kv_A values from ansatz 5.

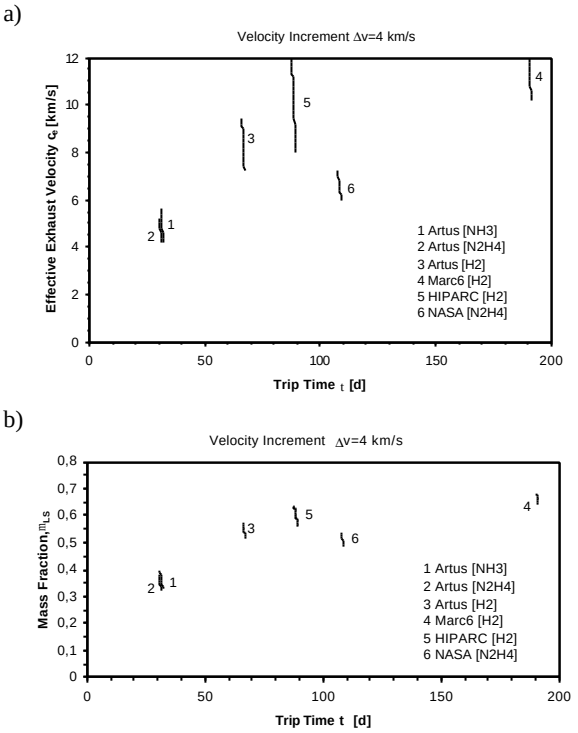

Fig. 13: Effective exhaust velocity c_e (a), payload and structure mass fraction μ_{LS} (b) vs. flight time τ for thermal arcjet thrusters in Table 3 for a velocity increment of Δv=4km/s

This can be explained with Fig. 9. Δv=0 also means that $\Delta v/c_e$=0, and therefore g_I must be equal to 1. For g_I=1, Eq. 7 can only be achieved with an exhaust velocity equal to kv_A. The experimentally verified regions where an optimization is possible are plotted with thick lines in Figs. 15a-d. For the applied field MPD thruster the optimal effective exhaust velocities considered here with the whole Δv region are far below the values which can be achieved with this lithium thruster.[28]

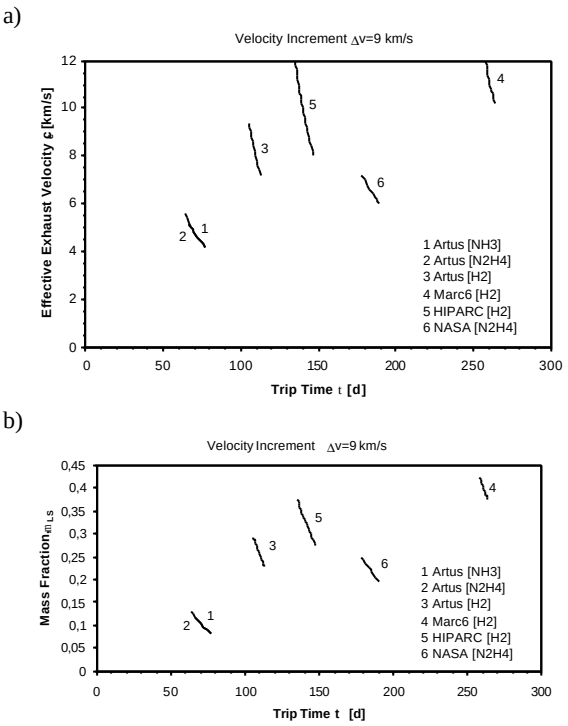

Fig. 14: Effective exhaust velocity c_e (a), payload and structure mass fraction μ_{LS} (b) vs. flight time τ for thermal arcjet thrusters (Table 3) for a velocity increment of Δv=9 km/s

From Fig. 15a it is visible that, for example, the Hall ion thruster SPT-100 only offers optimal effective exhaust velocities for velocity increments between 2.2km/s and 8km/s. If higher and lower Δv-values are required, the optimal exhaust velocities cannot be achieved as they are too low for low Δv's and too high in the case of high Δv's. Therefore, if one wants to use this thruster for a low Δv-mission (<2.2km/s) the lowest possible c_e should be used, in the case of a high Δv-mission (>8km/s), the highest c_e would be the best choice. These considerations lead to the thin lines in Fig. 15a. For the regions with a constant effective exhaust velocity the transport rate only depends on μ_{LS}. Therefore, Eq. 18 represents the only optimization condition and can be used for calculating μ_{LS} (thin lines in Fig. 15b). The corresponding flight time in this case can be calculated from the rocket equation 2 and leads to the thin lines in Fig. 15c.

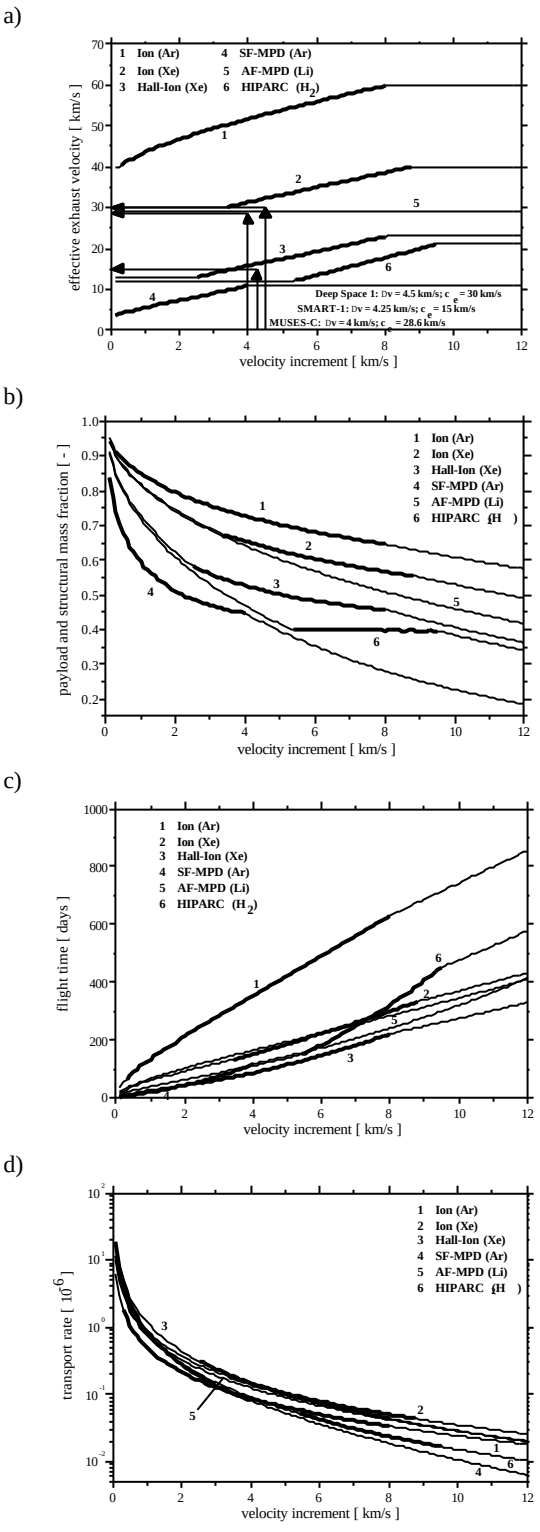

Fig. 15: Effective exhaust velocity c_e (a), payload and structure mass fraction μ_{LS} (b), flight time τ (c) and transport rate T_R (d) vs. velocity increments for the transport rate optimization for thrusters in Table 2

Also, the curves for the payload and structure mass fraction μ_{LS} (Fig. 15b) show behavior different from those of the preceding rocket equation optimization (Figs 11 and 12). The μ_{LS} values for the optimized region fall steadily from 1 to an asymptotical value determined by the maximal ratio of $\Delta v/c_e$ (see Fig. 9 and Eq. 18). The best payload fractions are achieved for the argon ion thruster (No. 1) due to its very high exit velocities, the worst for the self-field MPD thruster (No. 4) and the high power thermal arcjet (No. 6). The corresponding mission flight times τ, plotted in Fig. 15c, show quite a changed character. The lowest trip times can be achieved by using the self-field MPD thruster (No. 4) for low velocity increments up to 2.2km/s and the Hall ion thruster for high Δvs.

The optimization rate is defined so that it is large when a short flight time as well as a large payload fraction are achieved. Figure 15d makes it clear that for velocity increments up to 3.5km/s, the Hall ion thruster offers the highest transport rate due to its low loss factor. At velocity increments higher than 6km/s, the xenon ion thruster clearly takes over this good position due to its very high efficiency value. The self-field MPD thruster, which in contrast to the Hall ion thrusters and ion thrusters has not yet been optimized, is so far only preferable for very low velocity increments.

For three recent missions, Deep Space 1 (ion thruster Xe), SMART-1 (Hall ion thruster, Xe) and Muses-C (ion thruster, Xe), the effective exit velocities of each chosen thruster are included in Fig. 15a. The effective exhaust velocities agree quite well with the chosen operating points for the missions despite the simple transport rate model. Here the point must be made that the ion thrusters for both missions do not completely agree with thruster 2. Because the thrust efficiency dependence on exit velocity is not available or accessible to us for these devices, the correct calculation could not be performed.

The results for the optimization of the transport rate for the six selected thermal arcjet thrusters in Table 3 are displayed in Fig. 16. The experimentally verified regions where an optimization is possible are plotted with a thick line. Figure 10 has already shown that the optimal effective exhaust

a)

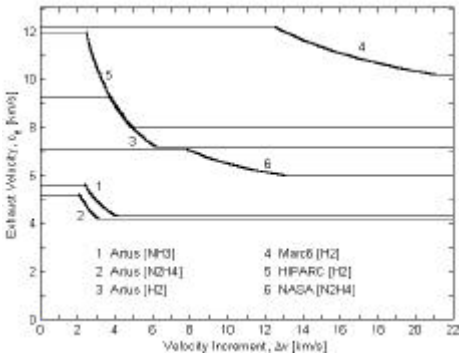

b)

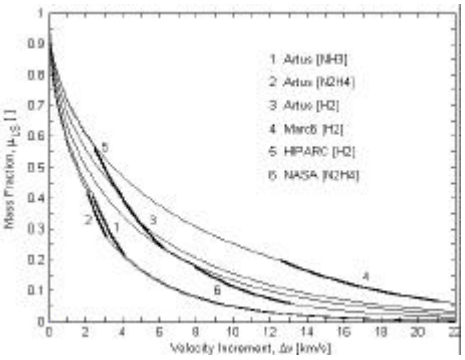

c)

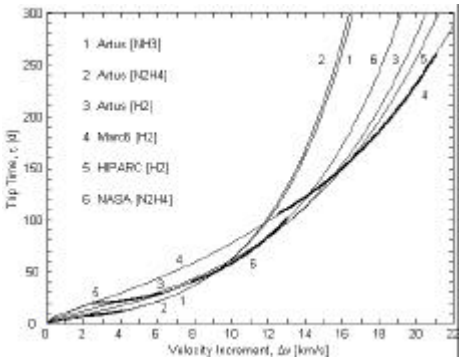

d)

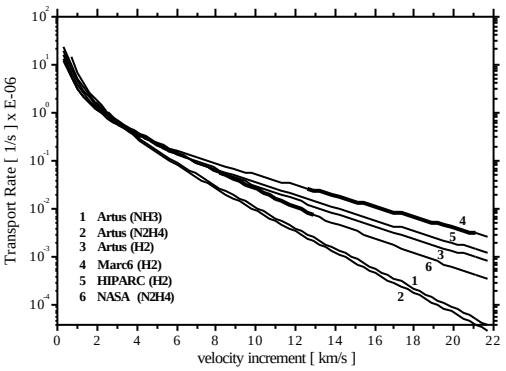

Fig. 16: Effective exhaust velocity c_e (a), payload and structure mass fraction μ_{LS} (b), flight time τ (c) and transport rate T_R (d) vs. velocity increment for the extended transport rate optimization for thrusters in Table 3

velocity for a specific Δv requirement now only depends on the parameter a/Δv. The same is true in view of Eq. 18 for μ_{LS}. The bigger a is, in other words the faster the exit velocity which corresponds to the energy content of the propellant which is not directly influenced by the arc, the larger the c_e required for an optimization and the larger the μ_{LS}. This means that improving the regenerative cooling capacity results in an increase of the payload and structure mass fraction. Fig. 16a shows how the optimal exhaust velocity decreases as the velocity increment increases within the optimization region. An optimization of the Marc 6 thruster with small velocity increments for example is not possible because the optimal c_e can no longer be achieved. This means that for a small velocity increment, the largest possible c_e should be chosen. If one, on the other hand, wants to use a thruster for a mission with a larger Δv requirement than its optimization area covers, it should be operated with the smallest possible c_e because then the higher efficiency (see Fig. 6) increases the transport rate. These considerations led to the thin lines in Fig. 16a. For the regions with a constant effective exhaust velocity the transport rate only depends on μ_{LS}. Therefore, Eq. 18 represents the only optimization condition and can be used for the calculation of μ_{LS} (thin lines in Fig. 16b). The corresponding flight time in this case can be calculated from the rocket equation 2 and leads to the thin lines in Fig. 16c. Generally speaking, the transport rate sinks as the velocity increment increases because the flight time (see Fig. 16c) as well as the payload and structure mass fraction (see Fig. 16b) drastically sink. This behavior is visible in Fig. 16d. Figure 16 shows that the smaller and likewise optimized thruster Artus is superior when the Δv requirement is small (<3km/s). For Δv>6km/s Marc 6 is superior due to its good regenerative cooling capacity. At this performance level, HIPARC can only be included in the comparison to a limited extent because it only has a relatively low regenerative cooling capacity, in which respect its stage of development and that of the thrusters Artus and Marc are not equivalent.

In Fig. 17 the transport rates of only four of the thrusters (two from each of the two groups discussed) are compared. Although the exhaust velocity which Marc 6 exhibits in the Δv region investigated is too low (compare Fig. 16a), its transport rate is superior to all the other thrusters when the entire region in considered. This is due to significantly shorter flight times which can be achieved. Here the large potential of the thermal arcjets is obvious.

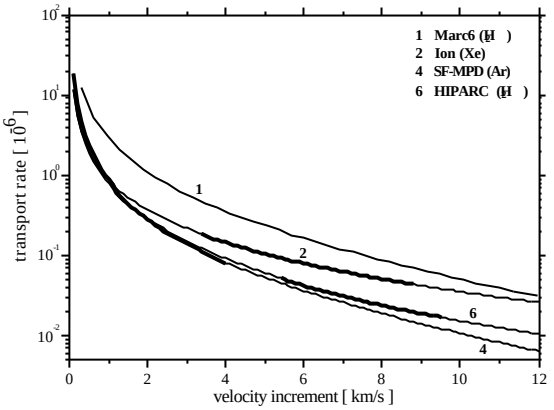

Fig. 17: Transport rate as a function of velocity increment [km/s] for selected thrusters

Through its optimal exhaust velocity, the high power arcjet HIPARC has already distinguished itself in the Δv region that is of interest for many missions. If it is possible to significantly increase HIPARC's efficiency through regenerative cooling and optimization, it would be of great interest for transfer and interplanetary missions.

Despite the high payload ratio that can be achieved with these thrusters, the Xe ion thruster's transport rate is significantly lower than that of Marc 6 because the flight time is very long due to the low thrust density that these thrusters exhibit. Significant improvements are no longer possible for these devices. For self-field MPD thrusters it is valid to say that their efficiency as well as their effective exhaust velocity must improve to make these devices competitive.

Conclusions

The purpose of this paper was the inclusion of the dependency of the specific power α_F on the exhaust velocity c_e into the flight mission parameter optimization and to show the tendencies of the results, not to give detailed solutions, for which the mass fraction division, for example, would not be refined enough. The results clearly show the strengths and weaknesses of individual thrusters and the influence of the propellant choice. In comparing the individual thrusters, one must keep in mind that the thrusters are in various stages of development. In some cases, there are already optimized and qualified thrusters (for example the Xe ion thruster, Hall ion thruster and low power arcjet and Marc 6). On the other hand, the regenerative cooling capacity of the HIPARC, for example, is far from exhausted and there are only simple laboratory models of the MPD thrusters.
In the case of the applied field MPD thruster, lithium is certainly not the best propellant choice because the effective exhaust velocity gets too high. If the exhaust velocity could be lowered, the transport rate would improve.[28] Certain important aspects in choosing the optimal thruster are not included in the optimization, such as the attainable thrust density lifetime, reliability and possible contamination. Despite the numerous simplifications, it could be shown for a number of current mission examples that the optimal effective exhaust velocities could be predicted fairly well.

Acknowledgments

We would like to thank Dr. Thomas Wegmann and Mr. Jörg Heiermann for their help with the figures and Ms. Jennifer Baer-Engel for typing and proofreading.

References

[1]Sovey, J., Rawlin, V., and Patterson, M., "Ion Propulsion Development Projects in U.S.: Space Electric Rocket Test I to Deep Space I," *Journal of Propulsion and Power*, Vol. 17, No. 3, pp. 517-526.

[2]Saccoccia, G., "European Activites in Electric Propulsion, *Proceedings of the 3rd International Conference on Spacecraft Propulsion*, Cannes, France, 2000, pp. 49-63.

[3]Toki, K., Kuninaka, H., Funaki, I., Nishiyama, K. and Shimizu, Y., "Development Status of a Microwave Ion Engine System for the Muses-C Mission," *Proceedings of the 26th International Electric Propulsion Conference*, Kitakyushu, Japan, 1999, pp. 753-760.

[4]Auweter-Kurtz, M., Gölz, T., Habiger, H., Hammer, F., Kurtz, H., Riehle, M. and Sleziona, C., "High Power Hydrogen Arcjet Thrusters," *Journal of Propulsion and Power*, Vol. 14, No. 5, 1998, pp. 764-773.

[5]Wegmann, T., Auweter-Kurtz, M., Habiger, H., Kurtz, H., and Schrade, H.O., "Experimental Comparison of Steady State Nozzle Type and Cylindrical MPD Thrusters at High Current Levels," *Proceedings of the 23rd International Electric Propulsion Conference*, Seattle, WA, USA, 1993, pp. 1124-1133.

[6]Rehder, J.J. and Wurster, K.E., "Electric vs Chemical Propulsion for a Large Cargo Orbital Transfer Vehicle", *Journal of Spacecraft and Rockets*, Vol. 16, Feb. 1974, p. 129.

[7]Kaufmann, H.R. and Robinson, R. J., "Electric Thruster Performance for Orbit-Raising and Maneuvering," *Progress in Astronautics and Aeronautics: Orbit-Raising and Maneuvering Propulsion – Research Status and Needs*, Vol. 89, edited by L.H. Caveny, AIAA, New York, 1984.

[8]Jones, R.M., "Comparison of Potential Electric Propulsion Systems for Orbit Transfer," *Journal of Spacecraft and Rockets*, Vol. 21, Jan. 1984, pp. 88-95.

[9]Regetz, J.D. and Terwilleger, L.H., "Cost Effective Technology Advancement Directions for Electric Propulsion Transportation Systems," *Progress in Astronautics and Aeronautics: Electric Propulsion and its Applications for Space Missions*, Vol. 79, edited by R.C. Finke, AIAA, New York, 1981.

[10]Masek, T.D and Ward, J.W., "Economics of Ion Propulsion for Large Space Systems", AIAA Paper 78-698, 1978.

[11]Silva, T.H. and Byers, D.C., "Nuclear Electric Propulsion System Utilization for Earth Orbit

Transfer of Large Spacecraft Structures," AIAA Paper 80-1223, 1980.

[12]Langmuir, D.B., "Low Thrust Flight: Constant Exhaust Velocity in Field-Free Space," *Space Technology*, edited by H.S. Seifert, Wiley, New York, 1959.

[13]Irving, J.H., "Low Thrust Flight: Variable Exhaust Velocity in Gravitational Fields," *Space Technology*, edited by H.S. Seifert, Wiley, New York, 1959.

[14]Stuhlinger, E., Ion *Propulsion for Space Flights*, McGraw-Hill, New York, 1964.

[15]Vondra, R.J. and Caveny, L.H., "Plasma Thruster Research in the U.S.A.," *Proceedings of the 17th International Electric Propulsion Conference*, Tokyo, Japan, 1984, pp. 20-27.

[16]Auweter-Kurtz, M., Kurtz, H.L. and Schrade, H.O., "Optimization of Electric Propulsion Systems Considering Specific Power as Function of Specific Impulse," *Journal of Propulsion and Power*, Vol. 4, No. 6, 1988, pp. 512-519.

[17]Kim, V., Garkusha, V., Murashko, V. Popov, G. and Tikhonov, V., "Modern Trends of Electric Propulsion Activity in Russia," *Proceedings of the 26th International Electric Propulsion Conference*, Kitakyushu, Japan, 1999, pp. 27-32.

[18]Auweter-Kurtz, M., *Lichtbogenantriebe für Weltraumaufgaben*, B.G. Teubner, Stuttgart, 1992.

[19]Bühler, R.D., "Plasma Thruster Development: Magnetoplasmadynamic Propulsion, Status and Basic Problems," AFRPL TR-86-013, Air Force Rocket Propulsion Laboratory, Edwards AFB, CA, 1986.

[20]Rawlin, V.K., "Operating of the y-Series Thruster Using Inert Gas", AIAA Paper 82-1929, 1982.

[21]Arhipov, B.A., Krochak, L.Z., Kudriavcev, S.S., Murashko, V.M. and Randolph, T., "Investigation of the Stationary Plasma Thruster (SPT-100) Characteristics and Thermal Maps at the Raised Discharge Power," AIAA Paper 98-3791, 1998.

[22]Tikhonov, V, Semenikhin, S., Brophy, J.R. and Polk, J.E., "The Experimental Performances of the 100kW Li MPD Thruster with an External Magnetic Field," *Proceedings of the 24th International Electric Propulsion Conference*, Moscow, Russia, 1995, pp. 718-724.

[23]Tikhonov, V, Semenikhin, S., Brophy, J.R. and Polk, J.E., "Performance of 130kW MPD Thruster with an External Magnetic Field and Li as a Propellant," *Proceedings of the 25th International Electric Propulsion Conference*, Cleveland, OH, USA, 1997, pp. 728-733.

[24]Riehle, M., Laux, T., Huber, F., Kurtz, H.L. and Auweter-Kurtz, M. "Performance Evaluation of Regeneratively Cooled 1, 10 & 100 kW Arcjets," *Proceedings of the 26th International Electric Propulsion Conference*," Kitakyushu, Japan, 1999, pp. 176-185.

[25]DARA Fkz 50-TT-9401, "Entwicklung eines 1 kW Hydrazin Triebwerk – Bericht der IRS Aktivitäten," Final Presentation, 1998.

[26]Curran, F.M. and Byers, D.C., "New Developments and Research Findings: NASA Hydrazine Arcjets," AIAA Paper 94-2463, 1994.

[27]Buden, D. and Garrison, P.W., "Design of a Nuclear Electric Propulsion Orbital Transfer Vehicle," *Journal of Propulsion*, Vol. 1, Jan. 1985, pp. 70-76.

[28]Auweter-Kurtz, M., "Optimization of Electric Thrusters for Primary Propulsion," AIAA Paper 01-3347, 2001.